Methanol decomposition to synthesis gas over supported Pd catalysts prepared from synthetic anionic clays

Ryuji Shiozaki [a,*], Takashi Hayakawa [b], Yan-yong Liu [a], Tomoko Ishii [a], Mikio Kumagai [a], Satoshi Hamakawa [b], Kunio Suzuki [b], Tatehiko Itoh [b], Tetsuya Shishido [c] and Katsuomi Takehira [c,*]

[a] *Chemical Technology Division, Institute of Research and Innovation, Takada 1201, Kashiwa, Chiba 277, Japan*
[b] *National Institute of Materials and Chemical Research, Tsukuba Research Center, AIST, Higashi 1-1, Tsukuba, Ibaraki 305, Japan*
[c] *Department of Applied Chemistry, Faculty of Engineering, Hiroshima University, Kagamiyama 1-4-1, Higashi-Hiroshima, Hiroshima 739, Japan*

Received 9 November 1998; accepted 22 February 1999

Supported Pd or Rh catalysts were prepared by the solid-phase crystallization method starting from hydrotalcite anionic clay minerals based on $[Mg_6Al_2(OH)_{16}CO_3^{2-}]\cdot 4H_2O$ as the precursors. The precursors were prepared by a coprecipitation method from the raw materials containing Pd^{2+} and various trivalent metal ions which can replace each site of Mg^{2+} and Al^{3+} in the hydrotalcite. Rh^{3+} was also used for preparing the catalyst as comparison. The precursors were then thermally decomposed and reduced to form supported Pd or Rh catalysts and used for the methanol decomposition to synthesis gas. Among the precursors tested, use of Mg–Cr hydrotalcite containing Pd^{2+} resulted in the formation of efficient Pd supported catalysts for the production of synthesis gas by selective decomposition of methanol at low temperature. Although Pd^{2+} cannot well replace the Mg^{2+} site in the hydrotalcite, the Pd supported catalyst (Pd/Mg–Cr) prepared by the solid-phase crystallization method formed highly dispersed Pd metal particles and showed much higher activity than that prepared by the conventional impregnation method. When the precursor was prepared under mild conditions, more fine particles of Pd metal were formed over the catalyst, resulting in high activity. It is likely that the high activity may be due to the highly dispersed and stable Pd metal particles assisted by the role of Cr as the co-catalyst.

Keywords: decomposition of methanol, synthesis gas, hydrotalcite, supported Pd catalyst

1. Introduction

Methanol is one of the largest volume commodity chemicals produced in the world and has drawn emerging attention as an alternative energy carrier as well as an important chemical feed stock [1]. Although liquid methanol is one of the most promising alternative automobile fuels from a non-petroleum source, its decomposition to CO and H_2 onboard a vehicle before being fed into the engine provides the ultimate method of using methanol as a clean and efficient fuel. Methanol decomposition to synthesis gas is also applicable for chemical storage of the waste heat in factories such as power stations and in iron manufacture, since the reaction is endothermic:

$$CH_3OH \rightleftharpoons CO + 2H_2 \quad \Delta H = 22 \text{ kcal mol}^{-1} \qquad (1)$$

Its equilibrium conversion reaches 100% at atmospheric pressure at 200 °C, however, catalytic activity is not sufficient at low temperature and catalyst deactivation is frequently observed [2]. Various metals are reported to be effective for this reaction [1–3], which are classified into two groups of catalysts: one is Cu-based catalysts such as Cu/ZnO or Cu/Cr_2O_3 [4–7], and the other is the group VIII elements such as Ni, Ni–Pt, Pt, Pd and Rh metals supported over SiO_2, Al_2O_3 or ZrO_2 [2,8–14]. For the purpose of realizing the process of methanol decomposition, the catalyst must be active at low temperature, selective at a wide range of temperature and sustainable during the reaction. ZnO or Cu/ZnO catalysts were often tested, because Cu/ZnO-based catalysts are industrial methanol synthesis catalysts. Although Cu/Zn/Cr oxide is a commercial methanol synthesis catalyst, its performance in the methanol decomposition reaction is poor [1,4–7]. In the cases of Cu- and Ni-based catalysts, the selectivity to synthesis gas is not sufficient due to the inevitable formation of methyl formate and methane, respectively, at low temperature below 250 °C. Among the precious metals, Pd seems to be preferred and its nano-particles prepared on ZrO_2 by the deposition–precipitation method fulfill the requirements [14]. The catalytic performances may strongly depend on the distribution and stability of metal particles on the surface of the catalyst.

Metal supported catalysts are conventionally prepared by wet impregnation of different supports. This method is not fully reproducible and may give rise to some inhomogeneity in the distribution of the metal on the surface. A new concept of catalyst preparation, therefore, may be required. Use of multi-component precursors might give rise to well dispersed and stable metal particles on the surface of oxide supports upon calcination and reduction. We have proposed a new method for the preparation of well dispersed and stable metal supported catalyst, i.e., "solid-phase crystallization" (*spc*). This method was successfully applied to the preparation of Ni supported catalysts for the partial oxidation and CO_2 reforming of CH_4 to synthesis

* To whom correspondence should be addressed.

gas by using perovskite-type mixed oxides as the precursors [15–18]. The *spc* method may be generally applicable in the preparation of highly dispersed metal supported catalysts starting from many kinds of mixed metal oxides as the precursors. A similar idea has been tested by using a hydrotalcite (HT) anionic clay as the precursor. Extremely dispersed Pt catalysts were prepared from $Pt(acac)_2$ and a Mg–Al mixed oxide, synthesized from a HT precursor [19]. Ni supported catalysts were prepared from a Mg–Al HT precursor containing Ni^{2+} and were tested in the hydrogenation of acetonitrile [20]. Highly dispersed Rh or Ni supported catalysts were prepared from Mg–Al HT anionic clay as the precursor and used for the partial oxidation of methane [21,22]. Here, we report the preparation of supported Pd catalysts from the hydrotalcite and the catalytic behaviors in the methanol decomposition to synthesis gas.

2. Experimental

2.1. Preparation of the catalysts

Catalysts were prepared by the *spc* method by using the HT anionic clays as the precursors. $[Mg_6Al_2(OH)_{16}CO_3^{2-}]\cdot 4H_2O$ (abbreviated as Mg_3Al_1) was used as the HT and a part of Mg^{2+} was replaced by Pd^{2+} for preparing the precursor of Pd supported catalyst. Rh^{3+} was also used for preparing the Rh supported catalyst by replacing the Al^{3+} site as a reference. Furthermore, Sc^{3+}, Cr^{3+}, Fe^{3+} and Ga^{3+} were used for replacing Al^{3+} sites to test the effect of trivalent metal ions in the HT precursors. The ionic radii of these trivalent ions are close to that of Mg^{2+} [23]. The HT precursors were prepared by co-precipitation at pH = 10.0 and at 90 °C, by adding slowly an aqueous solution (200 ml) containing the nitrates of the elements, if not specifically mentioned, to an aqueous solution (ca. 250 ml) containing NaOH (1 M) and Na_2CO_3. $Pd(NH_3)_2Cl_2$ was used as the Pd source, since crystallized Pd nitrate was not sufficiently soluble in water. After mixing for 40 min, followed by aging for one night at 90 °C, the resulting precipitate was filtered, washed with de-ionized water and dried at 100–105 °C for one night. The catalysts were obtained by calcining the HT precursors at 425 or 650 °C for 3 h in air, followed by reducing at 400 °C for 1 h in a 10 vol% H_2 in N_2 stream, and used as powders of particle size below 70 mesh (*spc*A). Some HT precursors were prepared by coprecipitation under almost the same conditions except that the mixing was carried out within 1 min at 10–12 °C followed by aging at 90 °C for 1 h, in order to obtain fine particles of metal species. The catalysts were obtained by calcining the HT precursors, followed by reduction and crushing in the same way as above. The latter method is denoted as *spc*B.

The Pd/MgO, Pd–Cr/MgO and Pd/Mg–Cr catalysts were prepared by the conventional impregnation method (*imp*) by using aqueous solutions of $Pd(NH_3)_2Cl_2$. MgO "smoke" powder (UBE Ind., Ltd., Japan, >99.98%; average particle size, 10 nm; surface area (BET), 167.8 $m^2\,g^{-1}$) and Mg–Cr HT (prepared by the co-precipitation method, followed by the calcination at 425 °C for 3 h) were used as the supports. The samples were treated at 425 or 650 °C for 3 h in air, and at 400 °C for 1 h in a 10 vol% H_2 in N_2 stream, and used as the catalysts for the reaction.

2.2. Catalytic reactions

The catalytic test was conducted using a fixed-bed flow reactor at 150–350 °C and at atmospheric pressure. 300 mg of the catalyst was sandwiched by quartz wool, packed in a ∅10 mm U-shaped quartz tube reactor, reduced at 400 °C for 20 min in a 10 vol% H_2 in N_2 stream, and then cooled down to room temperature in the same atmosphere. The reaction was started under a flow of 40 vol% methanol diluted with N_2 gas at the total flow rate of 10,000 ml h^{-1} g-cat^{-1} and at atmospheric pressure by increasing the reaction temperature from room temperature to 350 °C at the rate of 1.5 °C min^{-1}. During this temperature-programmed reaction (TPR), the temperature was held at 150, 200, 250, 300 and 350 °C, each for 1 h, where the catalytic activity was tested for each catalyst. The products were analyzed by three on-line TCD gas chromatographs. Molecular Sieve 5A was used for CO and H_2 analyses with He and Ar as the carrier gas, respectively. For the analyses of methanol, methyl formate (MF), dimethyl ether (DME) and CO_2, Polapak Q was used with He as the carrier gas. The selectivity of each product was calculated based on converted methanol.

2.3. Characterization of the catalysts

The metal compositions in the HT precursors and in the catalysts were determined by ICP analyses using a Thermo Jarrell Ash IRIS/AP. BET measurements were conducted by using a Shimadzu Micrometries Flow Sorb II 2300. X-ray diffraction (XRD) was measured by using a MAC Science MXP-18 diffractometer with Cu Kα radiation. Thermal analyses (TGA/DTA) were carried out by using Shimadzu DTA 50 and TGA 50 containing an electrobalance. Transmission electron micrograph (TEM) observation was carried out by using a Jeol JEM 2000FX equipped with a Hitachi/Kevex H-8100/DeltaIV EDS. The particle size of Pd metal was evaluated by using the Scherrer equation on XRD results and from TEM-EDS observation.

The dispersion and the surface area of Pd on the Pd supported catalysts were measured by the CO pulse method at room temperature. 20 mg of the catalyst was first reduced in 100 ml/min of H_2 at 400 °C for 20 min and then used for the measurements.

3. Results and discussion

3.1. Structure and activities of the Rh/Mg–M_{spcA} catalysts

Rh/Mg–Al_{spcA} catalysts were prepared by calcining the HT precursors of the composition $Mg_3Al_{1-x}Rh_x$

(x = 0.03, 0.17 and 0.33) at 425 or 650 °C and used in the methanol decomposition. The activity increased with increasing Rh content, and use of the composition $Mg_3Al_{0.67}Rh_{0.33}$ as the precursors resulted in the highest activity (figure 1). After drying at 100–105 °C, all the samples showed the XRD patterns of Mg–Al HT (JCPDS: 22-700). By calcining the samples at 425 or 650 °C, the lines of MgO (JCPDS: 3-998) alone were observed well coinciding with the results reported by Reichle [24]. According to the TGA analyses, the Mg–Al HT crystal structure was stable up to 275 °C and additional heating from 275 to 450 °C resulted in simultaneous loss of hydroxyl groups and carbonate as water and carbon dioxide, respectively. Even when the samples were heated at 650 °C, the hydrotalcite lattice was regenerated by the rehydration with carbon dioxide in water, as reported by Reichle [24].

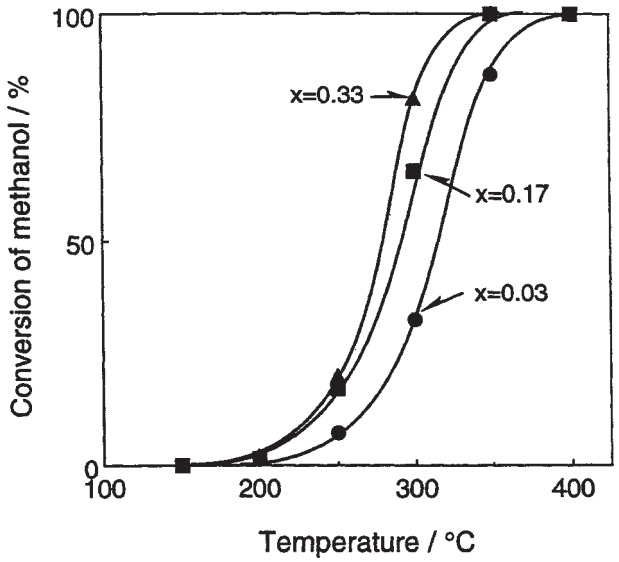

Figure 1. Decomposition of methanol over the catalyst prepared from $Mg_3Al_{1-x}Rh_x$ (x = 0.03, 0.17 and 0.33). The catalyst was calcined at 650 °C.

A series of Rh/Mg–M_{spcA} catalysts were prepared starting from the composition $Mg_3Rh_{0.33}M_{0.67}$ by using Al^{3+}, Sc^{3+}, Cr^{3+}, Fe^{3+} and Ga^{3+} as the M^{3+} ion and were tested in the methanol decomposition (table 1). Only the use of Cr^{3+} resulted in the formation of $MgCr_2O_4$ (spinel; JCPDS 10-351) together with MgO after calcination at 650 °C. Considering the high content of Rh and the absence of the lines of rhodium oxides in all the samples, Rh may be incorporated in the crystal structure of MgO, as reported by Basile et al. [21]. The calcination at low temperature (425 °C) caused an increase in the activity while a decrease in the selectivity to synthesis gas. Among the Rh/Mg–M_{spcA} catalysts tested, no significant difference was observed in the activity, i.e., 3–7% of methanol conversion was observed together with high selectivity to synthesis gas formation at 200 °C after calcination at 425 °C, except that use of Ga^{3+} as the M^{3+} ion resulted in the substantial formation of CO_2. A small amount of CO_2 formed over the catalysts containing Al^{3+}, Sc^{3+}, Cr^{3+} and Fe^{3+}. Neither CH_4 nor DME was observed, suggesting an occurrence of neither methanation (2) nor dehydration (3), respectively.

$$CO + 3H_2 \rightleftharpoons CH_4 + H_2O \quad (2)$$

$$2CH_3OH \rightleftharpoons CH_3OCH_3 + H_2O \quad (3)$$

A possible mechanism of CO_2 formation might be due to shift reaction (4) between CO and contaminated H_2O or reverse Boudouard reaction (5):

$$CO + H_2O \rightleftharpoons CO_2 + H_2 \quad (4)$$

$$2CO \rightleftharpoons CO_2 + C \quad (5)$$

3.2. Structure and activities of the Pd/Mg–M_{spcA} and the Pd/Mg–M_{spcB} catalysts

Use of Pd as the active metal resulted in the phase separation of PdO and MgO after calcination, although a smaller ratio of Pd/Mg was used compared to that of Rh/Mg. The composition $Mg_{2.84}Pd_{0.16}M$ (M^{3+} = Al^{3+},

Table 1
The analytical results and the catalytic activity of Rh/Mg–M_{spcA}.[a]

M	Atomic ratio Mg/M/Rh[b]	Calcination temp. (°C)	Phase observed	Conv. MeOH (%)	Select. (%)					
					CO	CH_4	CO_2	DME	MF	H_2
Al	6.00/1.49/0.70	425	MgO	5.9	98.4	0	1.7	0	0	100
		650	MgO	1.5	100	0	0	0	0	100
Sc	6.00/1.57/0.77	425	MgO	6.6	97.6	0	2.4	0	0	100
		650	MgO	5.5	100	0	0	0	0	100
Cr	6.00/1.50/0.73	425	MgO	6.8	98.1	0	1.9	0	0	100
		650	$MgO + MgCr_2O_4$	4.4	100	0	0	0	0	100
Fe	6.00/1.35/0.66	425	MgO	6.3	95.7	0	4.3	0	0	100
		650	MgO	5.4	97.6	0	2.4	0	0	100
Ga	6.00/2.10/0.70	425	MgO	3.4	63.6	0	36.4	0	0	100
		650	MgO	5.2	82.6	0	9.4	0	8.0	95.6

[a] IPC and XRD were used for the analyses. The catalysts were calcined at 425 or 650 °C and used at the reaction temperature of 200 °C. Precursor was dried at 105 °C.
[b] Atomic ratio calculated from the amount of reagents used was 6.00/1.32/0.66.

Table 2
The analytical results and the catalytic activity of Pd/Mg–M_{spcA}.[a]

M	Atomic ratio Mg/Pd/M[b]	Calcination temp. (°C)	Phase observed	Conv. MeOH (%)	Select. (%) CO	CH_4	CO_2	DME	MF	H_2
Al	5.60/0.23/2.00	425	MgO + PdO	7.1	100	0	0	0	0	100
		650	MgO + PdO	8.5	100	0	0	0	0	100
Sc	5.31/0.06/2.00	425	MgO + PdO	4.5	100	0	0	0	0	100
		650	MgO + PdO	10.4	100	0	0	0	0	100
Cr	5.00/0.13/2.00	425	MgO + PdO	10.3	100	0	0	0	0	100
		650	MgO + PdO + $MgCr_2O_4$	7.5	100	0	0	0	0	100
Fe	5.70/0.13/2.00	425	MgO + PdO	4.5	80.5	0	17.2	0	2.3	98.8
		650	MgO + PdO + $MgFe_2O_4$	5.2	87.6	0	8.7	0	3.7	97.9
Ga	4.34/0.10/2.00	425	MgO + PdO	3.1	95.2	0	4.8	0	0	100
		650	MgO + PdO	8.4	42.9	0	9.6	1.4	46.1	82.5

[a] IPC and XRD were used for the analyses. The catalysts were calcined at 425 or 650 °C and used at the reaction temperature of 200 °C. Precursor was dried at 105 °C.
[b] Atomic ratio calculated from the amount of reagents used was 5.68/0.32/2.00.

Table 3
The analytical results and the catalytic activity of Pd/Mg–M_{spcB}.[a]

M	Atomic ratio Mg/Pd/M[b]	Calcined at 425 °C	Surface area[c] (m^2 g-cat^{-1})	React. temp. (°C)	Conv. MeOH (%)	Select. (%) CO	CH_4	CO_2	DME	MF	H_2
Al	5.47/0.60/2.00	MgO + PdO	166	200	14.1	98.5	0	1.5	0	0	100
				300	95.9	98.8	0	1.0	0.3	0	99.8
Sc	4.74/0.59/2.00	MgO + PdO	139	200	16.8	96.9	0	3.1	0	0	100
				300	99.0	97.1	0.1	1.8	0	0	99.0
Cr	5.51/0.60/2.00	MgO + PdO	136	200	17.0	97.2	0	2.8	0	0	100
				300	97.7	98.9	0	1.1	0	0	100
Fe	5.25/0.59/2.00	MgO + PdO	86	200	7.8	84.1	0	13.2	0	2.7	98.4
				300	97.7	86.6	4.8	8.0	0	0	95.2
Ga	4.21/0.58/2.00	MgO + PdO	116	200	8.1	91.5	0	8.5	0	0	100
				300	78.1	98.2	0	1.3	0.6	0	99.6

[a] IPC and XRD were used for the analyses. The catalysts were calcined at 425 or 650 °C and used at the reaction temperature of 200 °C. Precursor was dried at 105 °C.
[b] Atomic ratio calculated from the amount of reagents used was 5.40/0.60/2.00.
[c] Reduced by H_2.

Sc^{3+}, Cr^{3+}, Fe^{3+} or Ga^{3+}) was used for preparing a series of Pd/Mg–M_{spcA} catalysts. The amount of Pd detected by IPC analyses was smaller than the value expected from the composition of raw materials, suggesting that Pd was not well incorporated in the catalyst by the *spc*A method (table 2). XRD studies of the catalysts showed the formation of HT in the precursors, MgO and PdO (JCPDS: 6-515) in the samples after calcination at 425 °C and MgO, PdO and mixed oxides after calcination at 650 °C. Thus it is likely that Pd^{2+} cannot well replace the Mg^{2+} site in the Mg–Al HT as the precursor. $MgCr_2O_4$ and $MgFe_2O_4$ (spinel; JCPDS: 17-464) were detected as the mixed oxides in the samples of Pd/Mg–Cr_{spcA} and Pd/Mg–Fe_{spcA}, respectively. Among the M^{3+} ions tested, Cr^{3+} and Sc^{3+} showed high activity for methanol decomposition, while Fe^{3+} and Ga^{3+} produced CO_2, DME and MF resulting in a decrease in the selectivity to synthesis gas. No formation of CH_4 was observed in all the reactions at 200 °C. The highest activity as well as the high selectivity to synthesis gas were observed over Pd/Mg–Cr_{spcA} and Pd/Mg–Sc_{spcA} calcined at 425 and 650 °C, respectively.

During the preparation of the precursors by the *spc*B method, mixing of raw materials at a low temperature and aging for a short time may suppress the growth of crystals, resulting in the formation of more fine particles of Pd metals in the catalysts. A larger amount of Pd was used in the *spc*B method and successfully incorporated in the catalyst, although Pd was still separated as PdO (table 3). All the catalysts prepared by the *spc*B method showed higher activities than those prepared by the *spc*A method. This may be partly due to the higher content of Pd and mainly due to the highly dispersed Pd metal particles as discussed later. The highest activity was again observed over the Pd/Mg–Cr_{spcB} and the Pd/Mg–Sc_{spcB} catalysts, among which the former showed better results than the latter at the low temperature of 200 °C. Moreover, use of Fe or Ga resulted in the formation of larger amounts of CH_4, CO_2 and MF. Use of Al or Ga resulted in the dehydration to form DME at high temperature. The surface areas of the catalysts were over 100 $m^2\,g^{-1}$ except for the Pd/Mg–Fe_{spcB} and an increase in the calcination temperature resulted in a decrease in the surface area.

Table 4
The analytical results and the catalytic activities of the Pd supported catalysts.

Catalyst	Pd/Rh (wt%)	Surface area[a] (m^2 g-cat^{-1})	Particle size of Pd[b] (nm)	React. temp. (°C)	Conv. MeOH (%)	Decomp. rate (mmol h^{-1} g-cat^{-1})	Select. (%)			
							CO	CH_4	CO_2	H_2
Pd/Mg–Cr_{spcA}	3.8	154	7.3 (7.2)	200	10.3	18.4	100	0	0	100
				300	89.6	160	99.8	0	0.2	100
Pd/Mg–Cr_{spcB}	14.6	136	∼3 (3–4)	200	14.6	30.6	97.2	0	2.8	100
				300	97.7	182	98.9	0	1.1	100
Pd/Mg–Cr_{imp}[c]	0.51	131	n.d.	200	2.8	5.0	99.2	0	0.8	100
				300	37.1	66.3	99.9	0	0.1	100
Pd/Mg–Cr_{imp}[c]	3.0	123	23.2 (16.8)	200	3.6	6.4	100	0	0	100
				300	39.1	81.0	100	0	0	100
Pd/MgO_{imp}[d]	3.0	36	19.0	200	1.0	1.8	100	0	0	100
				300	24.1	43.0	98.6	1.4	0	98.8
Pd–Cr/MgO_{imp}[d,e]	2.9	73	19.2	200	2.0	3.6	100	0	0	100
				300	47.6	85.0	100	0	0	100
Rh/Mg–Cr_{spcA}	17.4			250	27.4	48.9	99.2	0	0.8	100
				300[f]	53.5	143	95.4	3.2	1.3	94.2

[a] Before test.
[b] Calculated by using the Scherrer equation. Number in parentheses was obtained from TEM observation.
[c] Mg–Cr was prepared by calcining Mg–Cr HT at 425 °C for 3 h, BET surface area = 161 m^2 g-cat^{-1}.
[d] MgO was purchased from Ube Co., Ltd., particle diameter = 10 nm, BET surface are = 168 m^2 g-cat^{-1}.
[e] The amount of Cr was 2.9 wt%.
[f] Trace amount (0.1%) of dimethyl ether was formed.

3.3. Activities of the Pd/Mg–Cr_{spc} catalysts

The activities of the Pd/Mg–Cr_{spc} catalysts are compared with those of the Pd supported catalysts prepared by the impregnation method (table 4). The analytical results are also shown in the table where the loading of Pd was calculated by assuming that the Mg–Cr support is composed of MgO and Cr_2O_3. Among the Pd-impregnated catalysts, the Pd(3.0 wt%)/Mg–Cr_{imp} catalyst showed the best behavior. On the Pd/Mg–Cr_{imp} catalysts, the loading amount of Pd showed no crucial effect on the catalytic activity as seen in the results obtained by increasing the loading amount from 0.51 to 3.0 wt%. The Pd/MgO_{imp} catalyst showed quite a low activity, and a small amount of CH_4 was formed at 300 °C. Increasing the loading of Pd from 3.0 to 16.1 wt% in the Pd/MgO_{imp} catalyst resulted in the formation of CO_2. The surface area of MgO was 168 m^2 g-cat^{-1} as purchased and substantially decreased after the impregnation with Pd. Upon co-impregnation of Cr with Pd on MgO, the activity of the Pd–Cr/MgO_{imp} catalyst increased two times as high as the Pd/MgO_{imp}, while the formations of CH_4 and CO_2 were suppressed. Here, MgO was first impregnated with Cr followed by the impregnation with Pd, resulting in a two-fold increasing in the surface area of the Pd–Cr/MgO_{imp} compared to that of the Pd/MgO_{imp}. It is thus likely that Cr can work as a promoter for the Pd supported catalysts for the methanol decomposition into synthesis gas. The BET surface area of Pd/Mg–Cr_{spc} after the H_2 reduction at 400 °C for 1 h is 154 m^2 g-cat^{-1}, while that of Mg–Cr after the same treatment was 160 m^2 g-cat^{-1}, suggesting that the *spc* method can maintain the high surface area. Upon Pd impregnation, in contrast, a decrease in the surface area occurred as seen in 131 and 123 m^2 g-cat^{-1} for the Pd(0.51 wt%)/Mg–Cr_{imp} and the Pd(3.0 wt%)/Mg–Cr_{imp} catalysts, respectively. The presence of Cr in the impregnated catalyst system is still effective for attaining high activity, as seen in the results obtained over the Pd(3.0 wt%)/Mg–Cr_{imp} catalyst. All the Pd/Mg–Cr catalysts showed no activity for methanation (3) or dehydration of methanol (2) which are frequently observed as a side reaction in methanol decomposition over VIII transition metals or acid catalysts. The Rh/Mg–Cr_{spcA} as a reference did not show sufficiently high activity compared to the Pd/Mg–Cr_{spcA}, although the loading amount of Rh was higher than that of Pd. The selectivity to synthesis gas was low on the Rh catalyst.

3.4. Structure of the Pd/Mg–Cr_{spc} catalysts

XRD analyses of the Mg–Cr HT precursor containing Rh or Pd represent the typical diffraction pattern of HT, similarly to Mg–Al HT (JCPDS: 22-700), but with poor crystallinity resulting from the low synthesis temperature. Before the H_2 reduction at 400 °C, the Rh/Mg–Cr_{spc} catalyst gave only MgO diffraction peaks (JCPDS: 3-998), and no peak related to the Rh compound were detected. This may confirm the presence of Rh^{3+} ions inside of the MgO lattice [21]. In contrast, the Pd/Mg–Cr_{spcA} catalyst showed the additional diffraction peaks assigned to the PdO phase (JCPDS: 6-515), indicating that some of Pd ions segregated from the MgO cubic structure during the calcination treatment (figure 2). Just after drying at 110 °C, the lines due to the Mg–Cr hydrotalcite structure were observed although the crystallinity was not enough. By calcining the sample at 425 °C in air, the HT structure disappeared followed by the phase separation into PdO and MgO. XRD patterns of the Pd(3.0 wt%)/Mg–Cr_{imp} catalyst were also shown in figure 2 as a comparison. The PdO phase was reduced to Pd metal after the reaction in both cases. The Pd(0.51 wt%)/Mg–Cr_{imp} catalyst alone showed the peaks of neither PdO

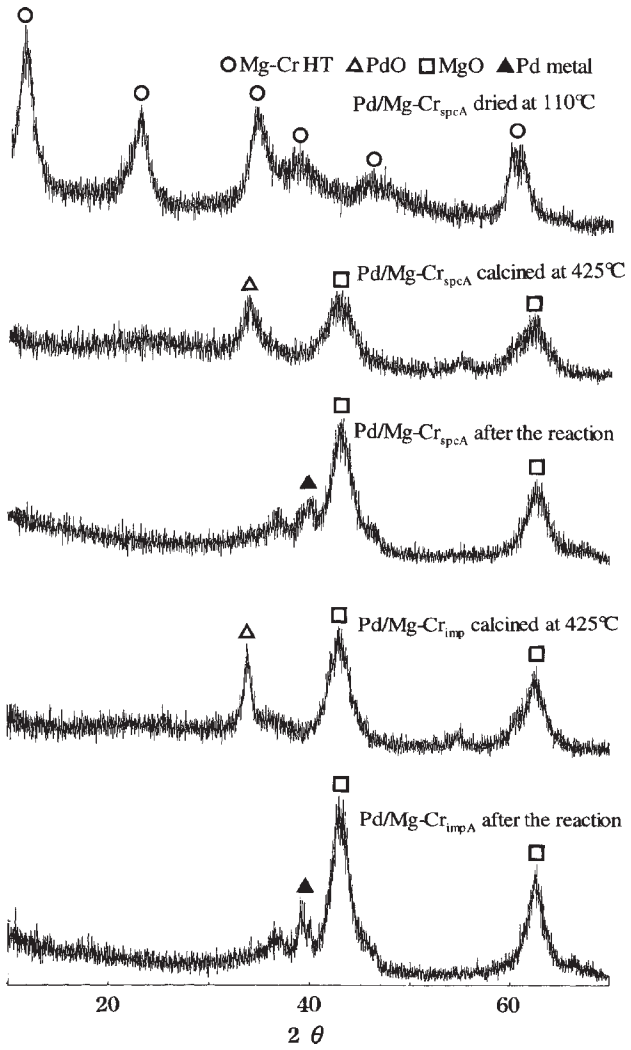

Figure 2. XRD patterns of the Pd/Mg–Cr_{spcA} catalyst before and after the TPR. The catalysts were calcined at 425 °C.

nor Pd metal. By using the Scherrer equation, particle sizes of PdO and Pd metal in the other catalysts were estimated from the PdO[101] and Pd[111] reflections at $2\theta = 33.9$ and 40.0°, respectively. The particle size of PdO in Pd/Mg–Cr_{spcA} is 6.6 nm, while those in Pd/Mg–Cr_{imp} are around 10 nm. After the H_2 reduction, the particle size of Pd metal increased on the impregnated catalyst on MgO, while no clear change was observed on Pd/Mg–Cr_{spcA} (*vide infra*). After the reaction, the catalysts containing both Pd and Cr showed the peak ($2\theta = 39.0°$) of Pd–Cr alloy [25], overlapping on the peak ($2\theta = 40.0°$) of Pd metal and resulting in no observation of the peak width of Pd metal.

TEM images of the Pd/Mg–Cr_{spcA}, the Pd/Mg–Cr_{spcB} and the Pd/Mg–Cr_{imp} catalysts before and after the catalytic test by TPR from 150 to 350 °C, respectively, are shown in figures 3–5. Black spots are attributed to the particles of Pd metal according to the EDS analyses and the particle sizes were measured on many spots, the number of which was 75 in each catalyst. The particle sizes of Pd metal can be put in the following order: Pd/Mg–Cr_{imp} > Pd/Mg–Cr_{spcA} > Pd/Mg–Cr_{spcB}, and the distributions of the particle size on Pd/Mg–Cr_{imp} and Pd/Mg–Cr_{spcA} before and after the catalytic test are shown in figures 6 and 7, respectively. A broad distribution (5–45 nm) was observed on Pd/Mg–Cr_{imp}, while a sharp one (5–15 nm) on Pd/Mg–Cr_{spcA}. Mean values of the particle size observed by the TEM are also shown in table 4. The sharp distribution

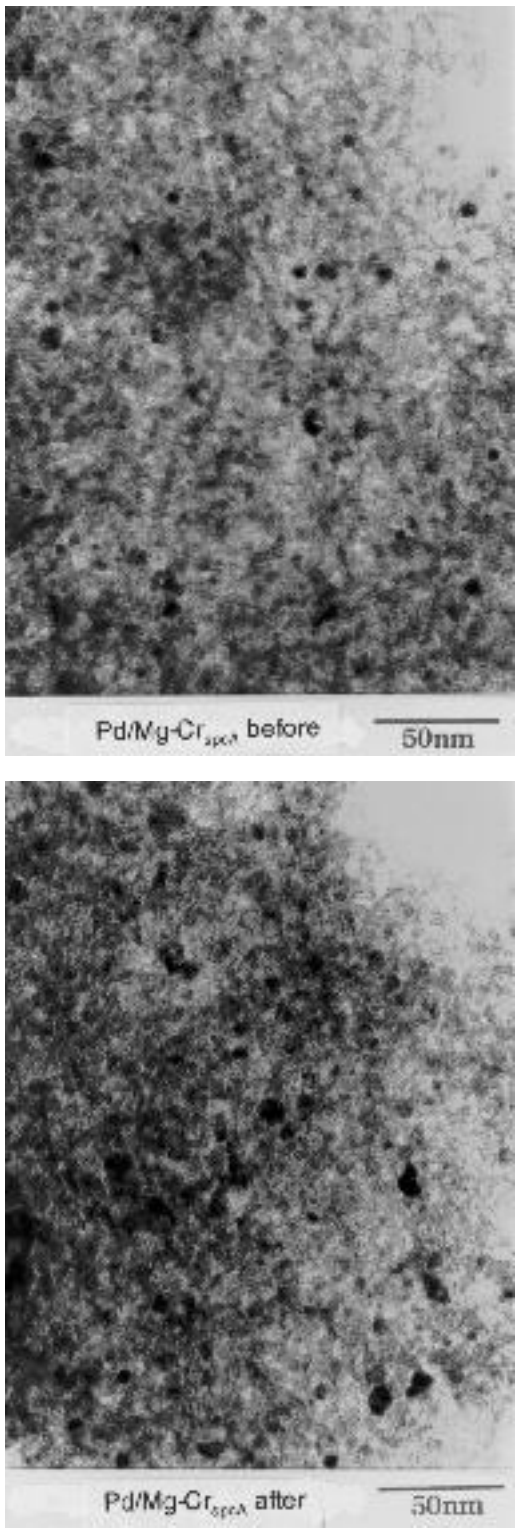

Figure 3. TEM images of the Pd/Mg–Cr_{spcA} catalyst before and after the TPR.

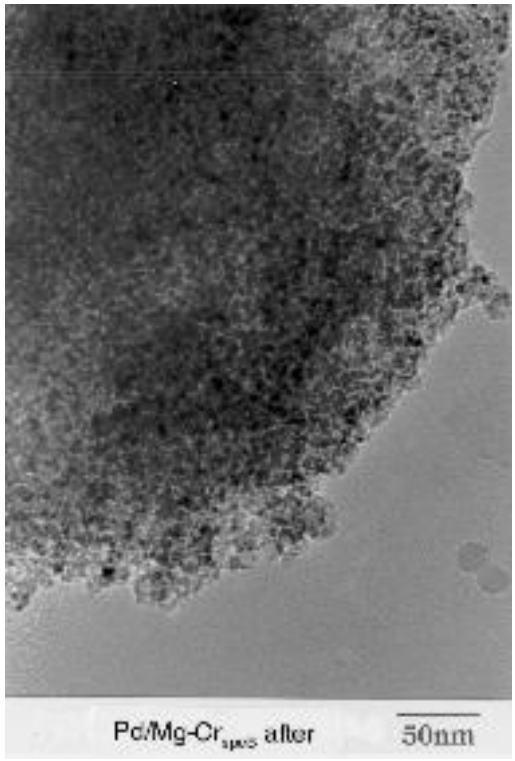

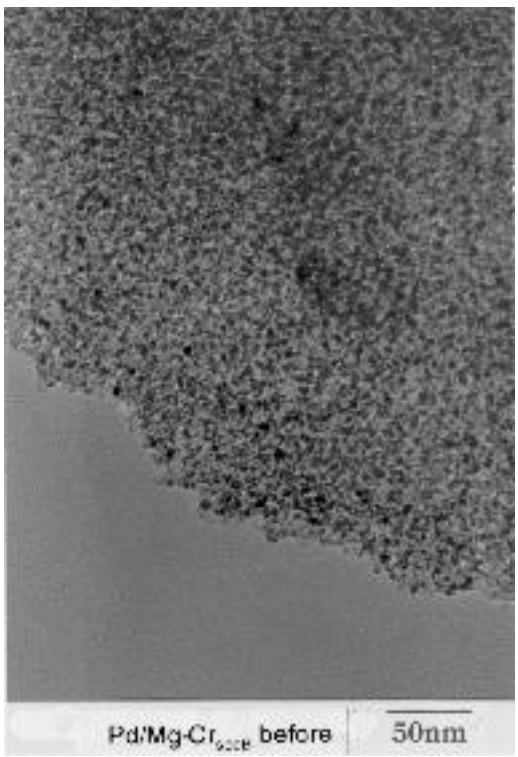

Figure 4. TEM images of the Pd/Mg–Cr_{spcB} catalyst before and after the TPR.

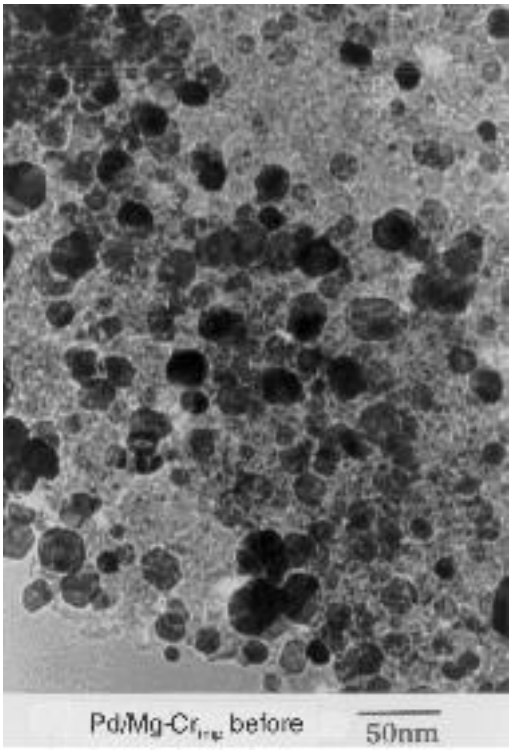

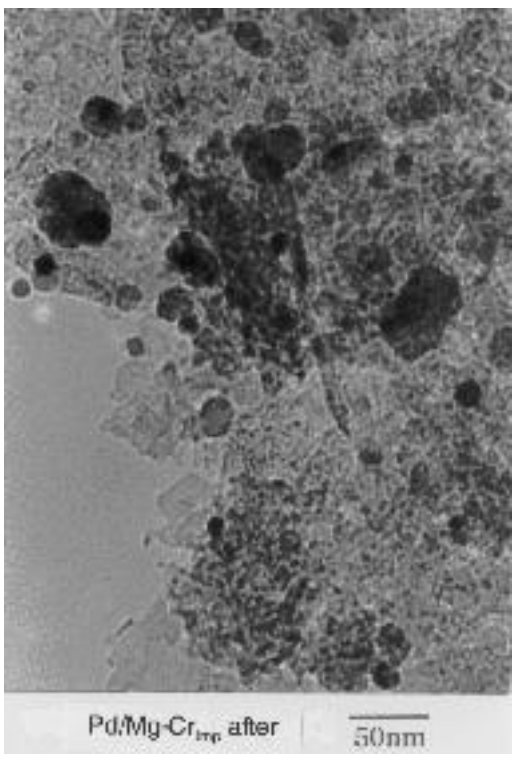

Figure 5. TEM images of the Pd/Mg–Cr_{imp} catalyst before and after the TPR.

of the small particle size on Pd/Mg–Cr_{spcA} did not substantially change (from 7.2 to 7.4 nm in average particle diameter) even after the catalytic test (figures 3 and 6), while the impregnated catalyst showed a clear change in the particle size distribution (from 16.8 to 19.2 nm) during the reaction (figures 5 and 7), suggesting that a sintering of Pd metals took place preferentially on the latter catalyst during the methanol decomposition. Pd metal particles on Pd/Mg–Cr_{spcB} were clearly observed only in the periphery of the catalyst particles and the size was estimated to be

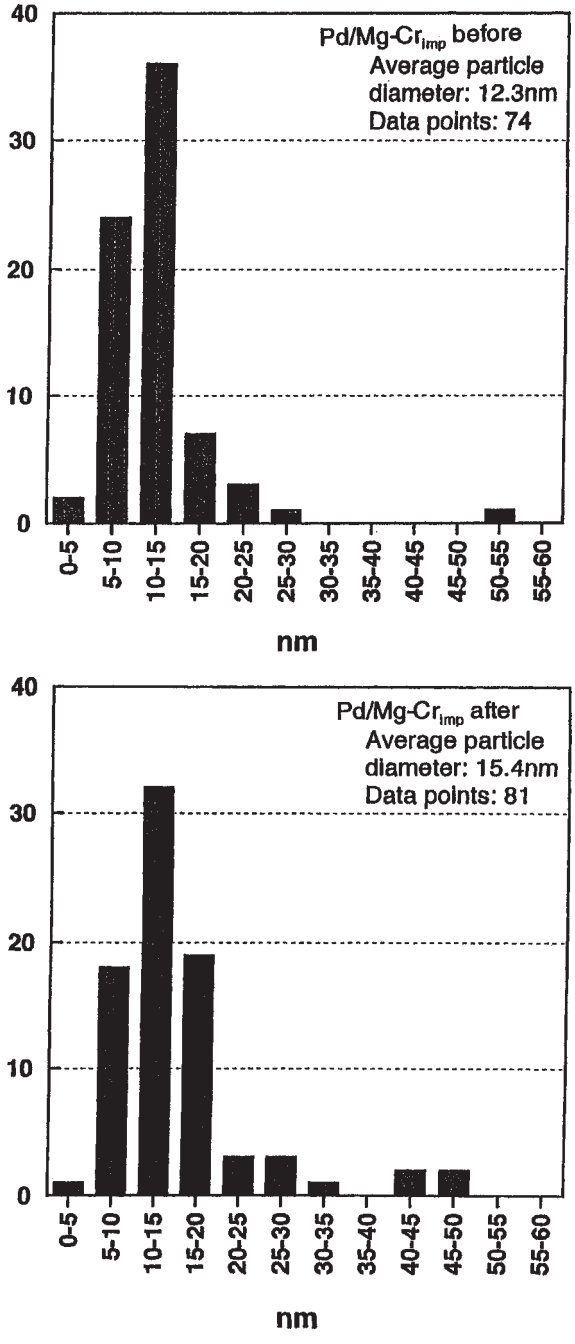

Figure 6. The distribution of the particle size of Pd metal on the Pd/Mg–Cr_{imp} catalyst before and after the TPR.

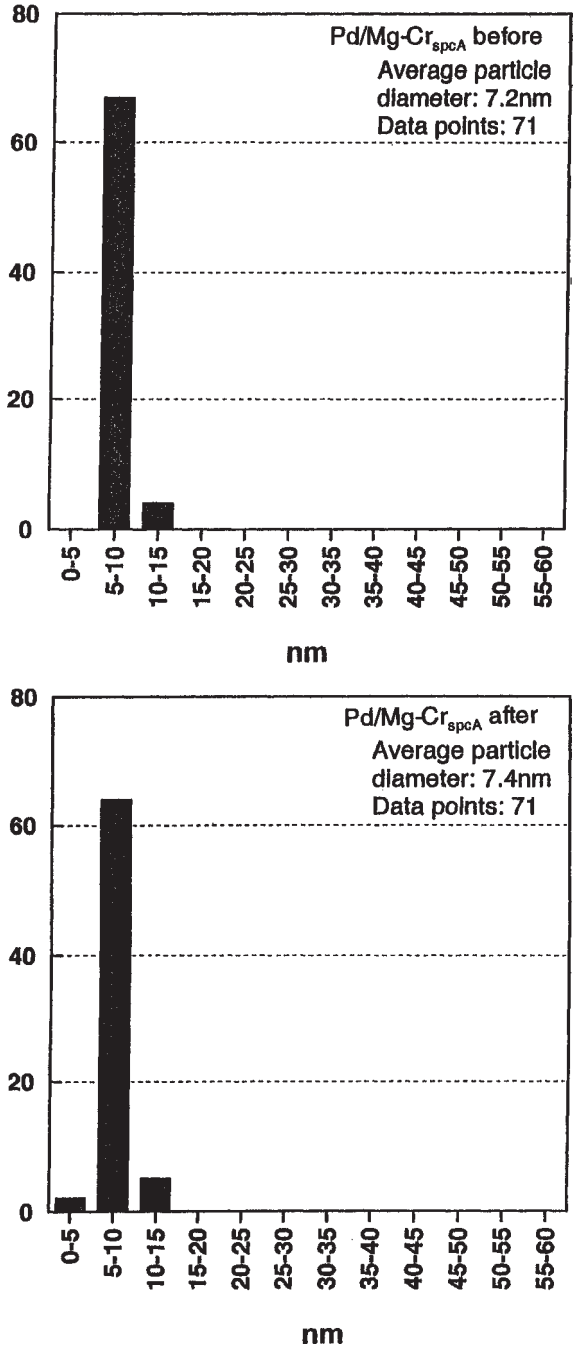

Figure 7. The distribution of the particle size of Pd metal on the Pd/Mg–Cr_{spcA} catalyst before and after the TPR.

3–4 nm (figure 4). The value obtained by the XRD data well coincided with that obtained by the TEM observation on Pd/Mg–Cr_{spcA} and Pd/Mg–Cr_{spcB}, while it is not the case on Pd/Mg–Cr_{imp} (table 4), i.e., a larger size of Pd metal particles was observed by XRD than by TEM. This may be due to the fact that a field of TEM observation was not sufficiently wide to cover all the particles of Pd metals, suggesting the presence of much larger size of Pd metal particles than observed in figure 5. Thus, it is likely that a well dispersed and stable Pd metal was formed by the *spc* method, resulting in the high activity for methanol decomposition into synthesis gas.

3.5. Kinetics of the methanol decomposition over the supported Pd catalysts

The rates of decomposition of methanol over the various supported Pd catalysts were plotted against the reaction temperature from 150 to 300 °C (figure 8). The highest rate as well as the lowest activation energy was again observed over Pd(3.8 wt%)/Mg–Cr_{spcA}, followed by the Pd(3.0 wt%)/Mg–Cr_{imp}, the Pd–Cr(2.9 wt%)/MgO_{imp} and the Pd(3.0 wt%)/MgO_{imp} catalysts. The loading amounts of Pd on these catalysts were almost comparable values

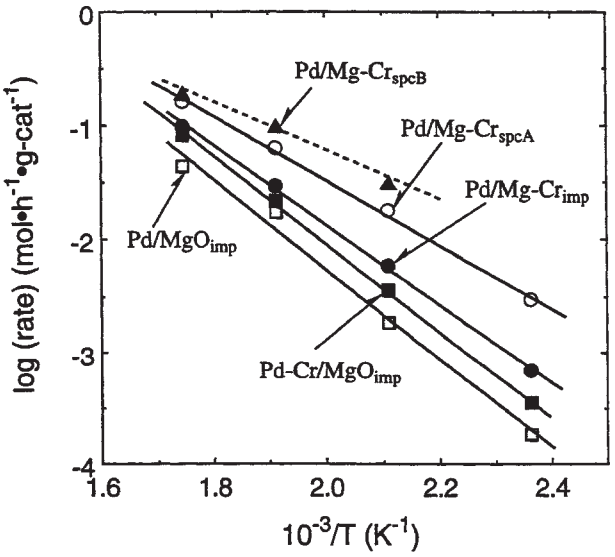

Figure 8. Arrhenius plot of rate of methanol decomposition over various Pd supported catalysts.

around 3.0 wt%. The apparent activation energies calculated from the data in figure 8 were 54.3, 67.2, 74.4 and 76.9 kJ mol^{-1} for the Pd(3.8 wt%)/Mg–Cr$_{spcA}$, the Pd(3.0 wt%)/Mg–Cr$_{imp}$, the Pd–Cr(2.9 wt%)/MgO$_{imp}$ and the Pd(3.0 wt%)/MgO$_{imp}$ catalysts, respectively. A value of 61.9 kJ mol^{-1} was obtained over Pd(0.51 wt%)/Mg–Cr$_{spcA}$, suggesting that the loading amount of Pd has no crucial effect on the activation energy. As a reference, the data obtained for the Pd(14.6 wt%)/Mg–Cr$_{spcB}$ catalyst were also shown as a dotted line in figure 8, where an apparent activation energy calculated exhibited a further lower value of 41.0 kJ mol^{-1}. Thus, the apparent activation energy of the methanol decomposition strongly depended on the preparation methods of the supported Pd catalysts and the presence of Cr as the co-catalyst. The activities of the catalysts Pd(3.8 wt%)/Mg–Cr$_{spcA}$ and Pd(14.6 wt%)/Mg–Cr$_{spcB}$ were again reproduced at 200 °C after the catalytic testing at 350 °C. This might be well supported by the fact that no significant sintering took place on these catalysts after the TPR (figures 3, 4 and 7).

Matsumura et al. [14] reported a lower apparent activation energy of ca. 80 kJ mol^{-1} over a 2 wt% Pd/ZrO$_2$ catalyst prepared by the deposition–precipitation method compared with that prepared by the impregnation method which produces the activation energy of ca. 100 kJ mol^{-1}. This was explained by the strong interaction between palladium nano-particles and zirconium oxide which may reduce the activation energy of the rate determining step in the methanol decomposition, i.e., decomposition of the surface methoxyl groups to surface carbon monoxide and hydrogen [26]. The value of the activation energy obtained in the present Pd catalysts prepared by the *spc* method in the presence of Cr was far lower than that obtained by Matsumura et al.

The dispersion and the surface area of Pd metal on the catalysts Pd(3.0 wt%)/Mg–Cr$_{imp}$, Pd(3.8 wt%)/Mg–Cr$_{spcA}$ and Pd(14.6 wt%)/Mg–Cr$_{spcB}$ were measured by the CO pulse method (table 5). In the *spc* method starting from mixed metal oxides as the precursors, the resulting catalysts may contain Pd metal homogeneously in the bulk. On the other hand, Pd metal may exist exclusively on the surface of the catalyst pepared by the *imp* method. Notwithstanding these considerations, the *spc* method afforded a higher value of both the dispersion and the surface area of Pd metal than the *imp* method. Moreover, the surface area of Pd metal on the Pd(14.6 wt%)/Mg–Cr$_{spcB}$ catalyst was still sufficiently high compared to the Pd(3.8 wt%)/Mg–Cr$_{spcA}$ catalyst, although the former contains almost four-fold larger amount of Pd compared to the latter. These facts clearly suggest that the *spc* method is preferable for the preparation of highly dispersed metal supported catalysts. It is most likely that the *spc* method is effective for affording the high activity as well as lowering the activation energy. This may be strongly due to the highly dispersed and stable Pd metal particles formed on the catalysts and the role of Cr as the co-catalyst.

Table 5
Dispersion and surface area of Pd metal on the catalysts.

Catalyst	Pd (wt%)	Dispersion of Pd (%)	Surface area (m^2 g-Pd^{-1})
Pd/Mg–Cr$_{spcA}$	3.8	13.1	64.6
Pd/Mg–Cr$_{spcB}$	14.6	13.6	66.9
Pd/Mg–Cr$_{imp}$	3.0	7.8	38.6

Acknowledgement

RS, YL, TI, and MK gratefully acknowledge a financial support from New Energy and Industrial Technology Development Organization.

References

[1] W.-H. Cheng and H.H. Kung, *Methanol Production and Use* (Dekker, New York, 1994) p. 1.
[2] K. Mizuno, Hyoumen 19 (1981) 513.
[3] T. Imai, Shokubai 28 (1986) 196.
[4] W.H. Cheng, S. Akhter and H.H. Kung, J. Catal. 82 (1993) 341.
[5] K.M. Tawarah and R.S. Hansen, J. Catal. 87 (1984) 305.
[6] A. Perrad, J.-P. Joly and J.-E. German, Bull. Soc. Chim. Fr. 1 (1984) 208.
[7] W.-H. Cheng, Appl. Catal. A 130 (1995) 13.
[8] S. Kasaoka and T. Shirakami, Nenryou-kyoukaishi 59 (1980) 40.
[9] H. Niiyama, M. Tamai, S. Kim and E. Echigoya, Sekiyu-gakkaishi 24 (1981) 322.
[10] K. Mizuno, Y. Iwasaki, T. Shu and M. Suzuki, Nenryou-kyoukaishi 60 (1981) 835.
[11] T. Imai, H. Fujita, K. Iida and S. Yokoyama, Shokubai 27 (1985) 136.
[12] S.R. Bare, J.A. Stroscio and W. Ho, Surf. Sci. 150 (1985) 299.
[13] Y. Matsumura, K. Kagawa, Y. Usami, M. Kawazoe, H. Sakurai and M. Haruta, J. Chem. Soc. Chem. Commun. (1997) 657.
[14] Y. Matsumura, M. Okumura, Y. Usami, K. Kagawa, H. Yamashita, M. Anpo and M. Haruta, Catal. Lett. 44 (1997) 189.

[15] T. Hayakawa, H. Harihara, A.G. Andersen, A.P.E. York, K. Suzuki, H. Yasuda and K. Takehira, Angew. Chem. Int. Ed. Engl. 35 (1996) 192.
[16] T. Hayakawa, H. Harihara, A.G. Andersen, K. Suzuki, H. Yasuda, T. Tsunoda, S. Hamakawa, A.P.E. York, Y.S. Yoon, M. Shimizu and K. Takehira, Appl. Catal. A 149 (1997) 391.
[17] R. Shiozaki, A.G. Andersen, T. Hayakawa, S. Hamakawa, K. Suzuki, M. Shimizu and K. Takehira, J. Chem. Soc. Faraday Trans. 93 (1997) 3235.
[18] S. Suzuki, T. Hayakawa, S. Hamakawa, K. Suzuki, T. Shishido and K. Takehira, Stud. Surf. Sci. Catal. 119 (1998) 783.
[19] Z. Gandao, B. Coq, L.C. de Menorval and D. Ticht, Appl. Catal. A 147 (1996) 395.
[20] F.M. Cabello, D. Ticht, B. Coq, A. Vaccari and N.T. Dung, J. Catal. 167 (1997) 142.
[21] F. Basile, L. Basini, G. Fornasari, M. Gazzano, F. Trifirò and A. Vaccari, J. Chem. Soc. Chem. Commun. (1996) 2435.
[22] F. Basile, L. Basini, M. D'Amore, G. Fornasari, A. Guarinoni, D. Matteuzzi, G. Del Piero, F. Trifirò and A. Vaccari, J. Catal. 173 (1998) 247.
[23] R.D. Shannon, Acta Crystallogr. A 32 (1976) 751.
[24] W.T. Richle, CHEMTECH (January 1986) 58.
[25] H. Baker et al., eds., *Alloy Phase Diagramms*, ASM Handbook, Vol. 3 (ASM International, 1992) pp. 2–156.
[26] T. Fukuhara, S. Sekiguchi, H. Muto and A. Igarashi, Kagaku Kogaku Ronbunshu 21 (1995) 1002.